City Research Online

City, University of London Institutional Repository

Citation: Bayat, M., Tsavdaridis, K. & Rodriguez, A. F. A. (2025). A Case Study for Optimising Geometry and Moment Capacity of Code Compliant Welded RWS Connections. Frontiers in Built Environment, 11, 1592665. doi: 10.3389/fbuil.2025.1592665

This is the accepted version of the paper.

This version of the publication may differ from the final published version.

Permanent repository link: https://openaccess.city.ac.uk/id/eprint/35205/

Link to published version: https://doi.org/10.3389/fbuil.2025.1592665

Copyright: City Research Online aims to make research outputs of City, University of London available to a wider audience. Copyright and Moral Rights remain with the author(s) and/or copyright holders. URLs from City Research Online may be freely distributed and linked to.

Reuse: Copies of full items can be used for personal research or study, educational, or not-for-profit purposes without prior permission or charge. Provided that the authors, title and full bibliographic details are credited, a hyperlink and/or URL is given for the original metadata page and the content is not changed in any way.

City Research Online: http://openaccess.city.ac.uk/ publications@city.ac.uk

A Case Study for Optimising Geometry and Moment Capacity of Code Compliant Welded RWS Connections

Meysam Bayat[1], Konstantinos Daniel Tsavdaridis[1]*, and Andres Alonso Rodrıguez[2]

[1]*Department of Engineering, School of Science and Technology, City St George's, University of London, Northampton Square, London, EC1V 0HB, United Kingdom*
[2]*Faculty of Engineering, Universidad la Gran Colombia, Bogotá, 110231, Colombia*

[*]*Corresponding author: Konstantinos.tsavdaridis@citystgeorges.ac.uk*

Abstract

A sustainable and resilient built environment requires structural solutions that minimise the use of high-environmental impact materials, while ensuring sound structural behaviour to extreme events. This study presents a seismic retrofit strategy employing reduced web section (RWS) connections to ensure inelastic behaviour initiates into the beam web within a designated protected zone, effectively protecting joints from stress concentration, while optimising the use of structural steel. RWS connections maintain flange integrity, allowing larger moment capacities to those cutting flanges while limiting out-of-plane instability to a greater extent. This method also allows for retrofitting from the level below, avoiding floor demolition. However, improper positioning or sizing of the web opening can lead to a non-compliant RWS connection compromising the capacity to withstand drift demands and altering the connection classification from fully restrained to partially restrained. To address these fine issues, this paper studies detailed finite element models aimed at optimising welded RWS connection designs subjected to AISC 341 loading protocol, while focusing on beam-column interface spacing and perforation diameter. This improves the state of the art by extending knowledge from bolted RWS to their welded counterparts, employing capacity design principles. Moreover, current literature lacks definitive guidance on optimal spacing and diameter ranges for RWS connections. This study addresses this gap by performing a parametric analysis of ninety finite element models with fixed boundary conditions in ABAQUS to identify the optimal geometrical parameters for Circular-cut RWS connections using IPE270 beams. The results show that specimens within the proposed range achieved ultimate drift demands over 4%, meeting AISC criteria for special moment frames with less than 20% strength degradation. The findings highlight that RWS connections are plausible solutions for seismic retrofit low-rise dwellings.

Keywords: Seismic Retrofit; Reduced Web Section (RWS); Seismic Steel Design; Special Moment Frames; Overstrength of RWS Connections.

1. Introduction

The construction of new steel structures exacerbates the climate crisis. According to the World Steel Association, the steel industry is responsible for approximately 7-9% of global direct CO2 emissions [1]. As such, retrofitting existing steel buildings is more sustainable and economical than demolition and new construction on many occasions [2]. Various studies have explored different retrofitting techniques and their effectiveness in enhancing existing buildings' structural integrity performance. Joint strengthening and beam weakening are the most widespread approaches for enhancing ductility and improving the behaviour of buildings to earthquake-induced ground motion [3] [4].

Reduced web section connection (aka RWS connection) is a beam-weakening strategy that allows for a protected region (i.e. the zone where inelastic action clusters away from locations where fragile behaviour could happen) by performing cuts in the beam web. This is practical in construction as access is only required from the floor below, thus avoiding slab demolition. Moreover, the laying of utilities and equipment is eased as they can go through the openings. Finally, the moment of inertia of the cross-section is larger overall compared to what is observed if the flanges are trimmed. Thereby, out-of-plane stability is less likely to happen [5].

The first approach for RWS in seismic design was Mark Amos Aschheim's patent in 2000 [6], which used web voids to create dissipative zones that function as structural fuses, preventing excessive stress at connections and enhancing the structure's seismic resilience. Comprehensive studies have further demonstrated that RWS connections can achieve high ductility and maintain stable hysteresis cycles, making them an efficient option for seismic retrofitting. This has been validated by both numerical simulations and laboratory testing [7] [8] [9] [10] [11] [12]. Similarly, Tsavdaridis et al. effectuated an experimental campaign showing how RWS connections outperformed RBS connections without seismic detailing, suggesting they may be more suitable for structural retrofitting in regions with low seismic hazard [13]. Furthermore, their studies showed that RWS connections on low-rise buildings can achieve stable hysteresis loops without significant strength degradation due to the simultaneous occurrence of the Vierendeel mechanism in the beams, protecting the beam-column connection. In Davaranpanah et al. experimental campaign, they compared RWS connections with RBS connections finding that the former achieved enhanced strength, stiffness, ductility, and lateral-torsional stability [5]. Tabar et al. showed that improved behaviour at meso-scale led to enhanced seismic performance of low-rise buildings. This was corroborated by effectuating incremental dynamic analyses on simulations having RWS and

RBS connections. They found that models furnished with limited-ductility RWS connections without capacity design principles have at least 25% lower chances of exceeding 1%, 2%, and 4% inter-story drifts than RBS connections within the same structure and with comparable detailing. Additionally, their collapse probabilities were one-third lower [14].

Although there are guidelines for assessing the structural capacity of beams with web openings subject to monotonic loads [15] [16], specifications for design considering earthquake actions for moment frames are lacking, regardless of ample evidence of the capabilities of RWS for enabling stable inelastic action. For example, the Recommended Seismic Design Criteria for New Steel Moment Frame Buildings (SAC Joint Venture), also known as FEMA 350, focuses on prequalified connections that modify the beam's flanges or strengthen the beam-column connection using plates [3]. However, RWS connections are not prequalified in the guidelines yet and is highlighted that “an understanding of the utility of this system for enduring seismic actions is developing” [3]. This study contributes to addressing this knowledge gap by performing a parametric assessment of the behaviour of welded RWS connections, considering different geometric configurations, a first critical step for prequalification.

Although there has been previous research about the seismic behaviour of welded RWS, including both numerical simulations and experimental assessments that reiterate the capacity of these contentions to endure cyclic demands expected from earthquake actions, attaining a performance comparable to their bolted counterparts. However, these assessments considered a few numbers of specimens, and they did not address overstrength characteristics or propose geometric constraints to enforce capacity design principles.

Consequently, this study aims to perform a parametric analysis of welded RWS connections for low-rise buildings. They will be based on detailed finite element (FE) simulations of 90 specimens subjected to prequalification testing protocols following AISC guidelines. Henceforth, this paper is structured as follows; firstly, overall characteristics of the behaviour of seismic steel connections are introduced in Section 2, making emphasis on the prequalification process. Then, properties of the expected behaviour of ductile RWS connections are discussed in Section 3, particularly highlighting the expected failure mechanism of the connection. Section 4 presents the validation protocol of the simulations, which focused on the replication of tests performed on welded steel connections. Section 5 presents the procedure for the parametric assessments along with the most relevant results. Finally, the work is wrapped in the conclusions, where the most significant results are

summarised, along with introducing the limitations of the scope of the study and further research.

2. Prequalification Framework for Seismic Resiliency of Steel Moment Frame Connection

Prequalification is the most widespread approach for demonstrating compliance of steel connections with performance targets set up by specifications [17]. It involves real-scale testing of connection specimens following a pre-defined demand protocol. These demands are imposed displacements at inflexion points of columns representing interstorey drift demands. The AISC testing protocol is shown in **Figure 1**. It is the most widely used prequalification protocol [17], but there are currently alternatives being developed to represent seismic demands in Europe [15].

Particularly, the following characteristic ordinates are of interest. (i) Effective yielding, which corresponds to the onset of appreciable structural damage leading to non-reversible deformation. In the AISC guideline [17], it is the ordinate of the moment-rotation backbone hysteresis curve where the specified yielding moment of the connection is reached. (ii) Maximum moment capacity, corresponding to the largest moment recorded during the imposed cyclic drift demands up to the maximum applied drift, 6% (at which the analyses stop). (iii) The ultimate moment, namely the moment and drift ordinates for which vertical load carrying capacity is compromised, or moment decreases by 20% from the maximum moment capacity. An outline of the backbone curve, i.e., the envelope of the typical hysteretic response of a moment connection is shown in **Figure 2**.

Number of cycles	Rotation (rad)
6	0.00375
6	0.005
6	0.0075
4	0.01
2	0.015
2	0.02
2	0.03
2	0.04
2	0.05
2	0.06

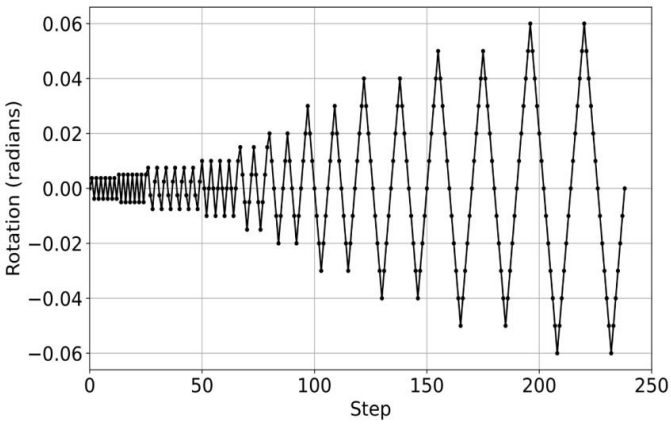

Figure 1: AISC 341 loading protocol *[17]*

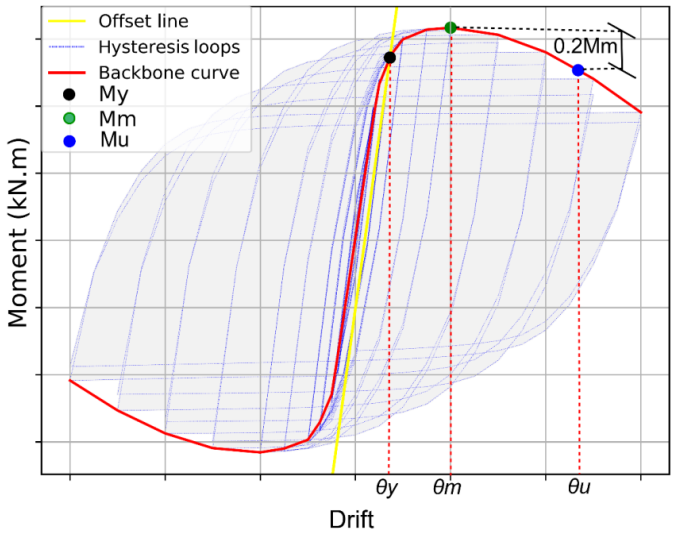

Figure 2: Typical backbone curve for characterising the response of a steel connection, following AISC 341

A connection within an intermediate moment resisting frame is required to reach a 0.02 ultimate interstorey drift demand, whereas a minimum 0.04 ultimate interstorey drift demand must be attained for deployment within a special moment resisting frame (SMF) [17].

3. Ductile Mechanisms of a Welded RWS Connection

RWS connections aim at clustering inelastic action by weakening the cross section after making perforations on the beam's web. Henceforth, capacity design must be enforced to preclude damage elsewhere. The column, the panel zone at the intersection of the beam and column, connecting welds and the vicinity of the column-beam interface are critical locations. The overall geometry of a welded RWS connection with RWS geometry parameters is shown in **Figure 3**.

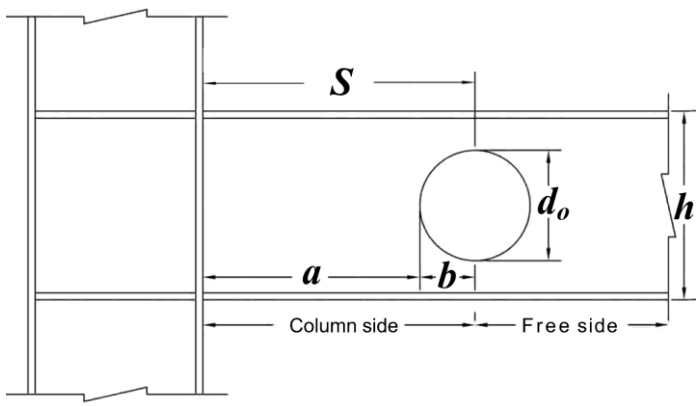

Figure 3: RWS connection geometry

The first ductile mechanism of an RWS connection is the complete yielding of the reduced cross-section, as shown in **Figure 4**. The cross-section deforms according to Euler-Bernoulli's plane section hypothesis, leading to compression at the bottom leg, while tension at the upper one. Hence, moment capacity is given by:

$$M_{P1} = \left(Z - \frac{d t_w^2}{4}\right) f_y \tag{1}$$

Where M_{P1} is the plastic moment of the reduced cross-section, Z is its plastic modulus, t_w *is* the beam's web thickness, and f_y is the yielding strength of the steel. However, reaching this plastic modulus requires effective transfer of shear across the perforation, (**Figure 5**), namely:

$$M_{Ptee} > V \frac{d_o}{8} \tag{2}$$

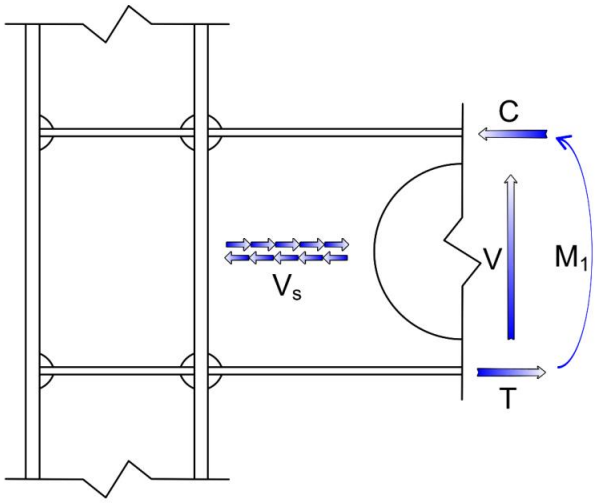

Figure 4: Full plastification of the reduced cross-section

As moment demands are taken in the middle of the symmetric Tee stubs (**Figure 5**), V describes the shear at the centre of the perforation. If moment capacities of the tee stubs (M_{pTee}) at the edge of the perforation are less than the value prescribed by Equation (2), the moment capacity will become lower than what corresponds to the full plastification of the reduced cross-section, leading to the Vierendeel mechanism. In this case, capacity will be controlled by yielding the tee stub sections. Nevertheless, yielding of the reduced cross-section and inelastic action on the edges of the perforation are usually concurrent.

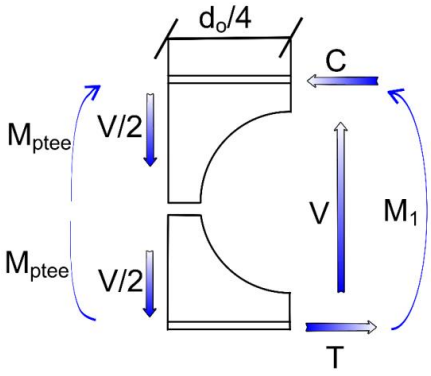

Figure 5: Equilibrium of T Stubs

Also, it is possible that the Euler-Bernoulli plane hypotheses don't hold for the whole cross-section, leading to strain incompatibility between the sections outside the opening (**Figure 6**). Namely, both upper and lower tee sections will observe both compressive and tensile strains, as sections of two beams stacked together, having only the same deflections.

$$2M_{p2} > 2Z_{Teer}f_y \tag{3}$$

In this case, moment capacity is given by Equation (3), where Z_{Teer} is the plastic section modulus of each of the tees right over the centre of the perforation.

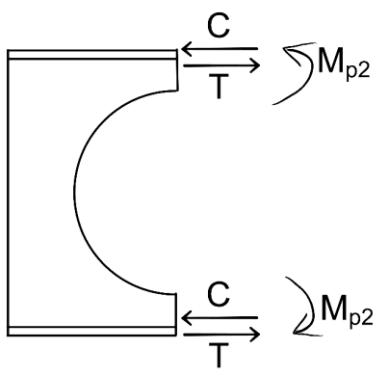

Figure 6: Yielding with relative sliding on both tees of the cross-section

However, other fragile mechanisms are possible. Being the most critical local flange bucking and web crimpling. The first is a consequence of failure in compression of the upper tee (**Figure 3**) when subjected to sagging moments. The same phenomenon is observed in the bottom tee when the moment reverses. The second is caused by an insufficient beam web thickness to efficiently transfer shear induced by tension and compression actions across the cross-section, away from the perforation. These undesirable failure modes can be mitigated if Equation (4) holds:

$$C + \frac{4M_p}{h-d_0}\frac{2S}{L-2S} > V_s = 0.3 f_y t_w (2s - d_o) \quad (4)$$

Capacity design can be enforced to ensure that connection elements away from the perforation remain elastic. This is done by performing checks for axial, and shear demands considering increased moments by the overstrength factor that consider strain hardening, provision of stronger-than-expected materials and inelastic load redistribution. The factor by which design moments are increased for performing these checks is called the overstrength factor [28]. In this study, factors related to load redistribution will be assessed, by considering the results of detailed FEMs of connection specimens.

4. Methodology

The behaviour of beam-to-column joints can be evaluated with the aid of the component method, largely adopted in research and incorporated into the Eurocode 3 (EC3) [18]. From a theoretical point of view, it can be applied to any connection, provided that the primary sources of strength and deformation are appropriately identified and modelled [19]. The component method considers the individual components of the connection, such as the beam, column, end plate, bolts, and welds, and analyses their behaviour and interactions within the whole connection. Breaking down the connection into its constituent parts helps to understand the complex behaviour of connections under various loading conditions, thus easing the formulation of design guidelines [18]. Following the objectives of this study, we deliberately modelled the beam with fixed ends, assuming an infinitely strong panel zone, to strip away the beneficial flexibility of the column and panel zone and thereby isolate the influence of the reduced-web-section (RWS) geometry on cyclic response; this yields a conservative upper-bound on plastic rotations and drift demands.

Other researchers like Mojtabaei et al. [20] have validated this approach, Phan et al. [21], Ye et al. [22], and Horton et al. [23] [24] [25]. This ensures that changes in response are due to alterations in RWS geometry, providing clear insights into its behaviour under seismic cyclic loading. Later, where frame-level estimates are required, the additional rotation of the joint components can be superimposed using the EC3 component method [18], ensuring that the conclusions of our 90-specimen parametric study remain applicable once realistic joint flexibility is reintroduced.

In this study, a numerical framework developed in ABAQUS and Python, which was benchmarked against two experimental studies [5] [26]. Then, ninety model assessments were

made on a beam fixed (rotation-constrained) on a column. Interstorey drift demands are lower-bound capacity estimates, as column and panel zone deformations are neglected.

Key focus areas include identifying combinations of S and d_o where yielding is confined to the protected zone around the perforation, thus supporting capacity design. The analysis also defined scaling factors to characterise the connection's moment capacity relative to the plastification of the reduced cross-section, leading to the formulation of overstrength factors related to load redistribution. The overall methodology is shown in **Figure 7**.

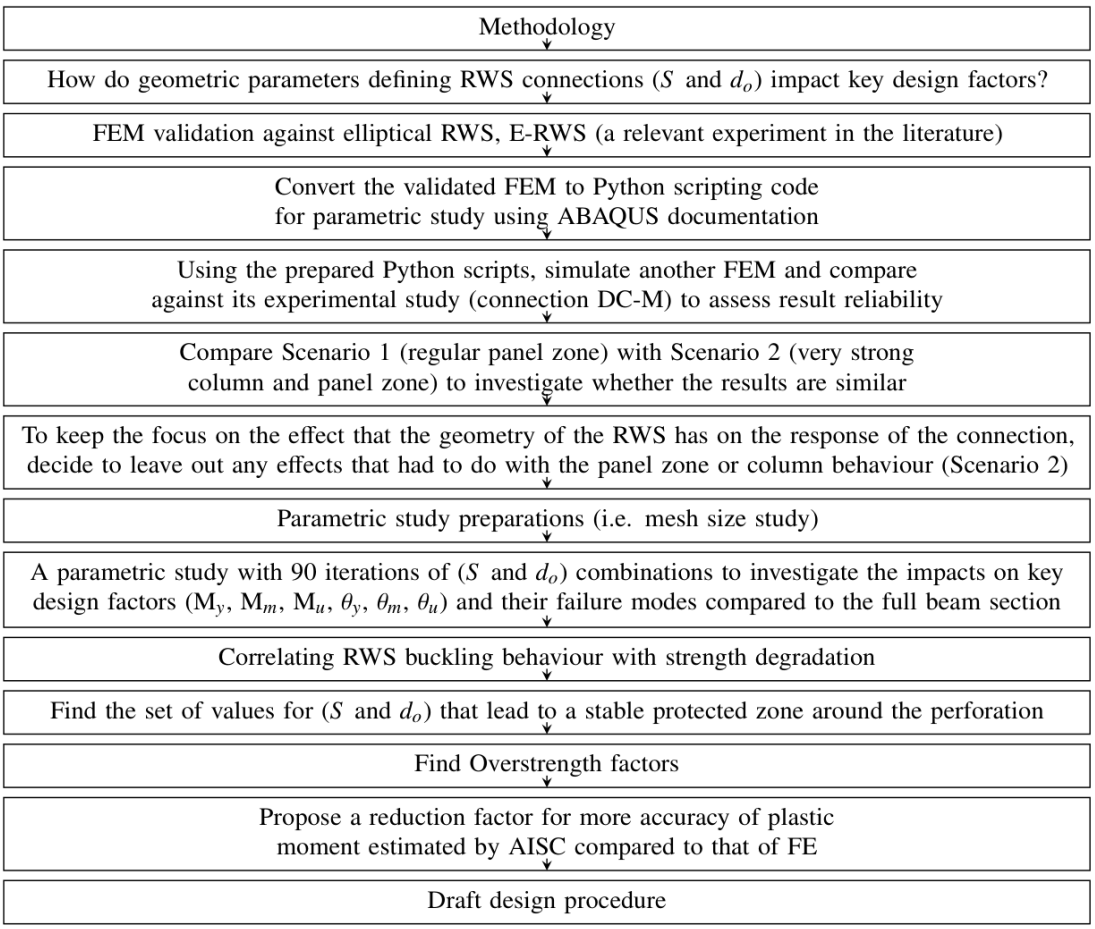

Figure 7: Flowchart illustrating the methodology used in this study

4.1 Validation of FE models

This study considered two full-scale sub-assemblies previously investigated experimentally to validate the proposed framework by generating FE models in ABAQUS. Davarpanah et al. [5] studied the cyclic behaviour of RWS (HE-RWS) connections with elliptical web openings, while Nia et al. conducted two identical experimental investigations on the Welded Unreinforced Flange-Welded Web connection to box columns under biaxial bending under the name (DC-M-1 and DC-M-2) models [26]. The cyclic load applied in both experiments

followed the AISC/ANSI 341-16 loading protocol. Details of both experiments are tabulated in **Table 1**, and further information can be found in [5] and [26].

Table 1: Detail of HE-RWS and DC-M connections from experimental tests (F: Flange, W: Web, L: Length, D: Depth, B: Breadth, L: Length) & (*v in all models equals to 0.3)*

Test	Section/Part	Thickness (mm)	Dimensions (mm)	Young's Modulus (GPa)	Yield Stress (MPa)	Ultimate Stress (MPa)	Elongation (%)
HE-RWS	IPE270 Beam	F: 10.2 W: 6.6	D: 270 B: 135 L: 1070	F: 196.0 W: 191.3	F: 265.1 W: 250.3	F: 405.3 W: 398.4	F: 24.2 W: 27.6
	IPB200 Column	F: 15.0 W: 9.0	D: 200 B: 200 L: 1500	F:198.7 W: 196.3	F: 286.6 W: 295.5	F: 415.8 W: 403.2	F:23.5 W: 25.6
	Doubler Plates	10.0	370×150	196.5	265.1	405.3	24.2
	Continuity Plate	10.0	170×87	196.5	265.1	405.3	24.2
	Stiffeners	12.0	249×64	196.5	265.1	405.3	24.2
DCM-1 & DCM-2	Beam	F: 15 .0 W: 8.0	D: 330 B: 240 L: 2500	201.0	F: 351.0 W: 252.0	F: 482.5 W: 399.6	F: 27.5 W: 30.8
	Box column	Plate: 20.0	D: 400 B: 400 L: 3000	201.0	252.9	364.3	35.0
	Continuity Plate	25.0	360×348	201.0	252.5	321.6	32.3
	Shear Plate	8.0	260×100	201.0	351.0	482.5	27.5
	Stiffeners	8.0	300×116	201.0	351.0	482.5	27.5

4.2 Overall properties of the FEM models employed in this study

The steel behaviour is modelled using a trilinear stress-strain curve with combined hardening for all elements. Full 3D nonlinear static analyses were effectuated, using the Newton-Raphson algorithm as the numerical solver within ABAQUS. This approach effectively accounted for nonlinearities arising from large displacements and deformations while neglecting inertial effects on the specimen. Additionally, 4-node reduced integration shell (S4R) elements were employed to enhance computational efficiency and accurately capture local buckling behaviour observed in both the beam web and flanges. Out-of-plane displacements are restricted by providing lateral support at boundaries. Sensitivity studies of the configuration and the density of the FE mesh size led to an optimal element size of 15mm. The welding line was not explicitly modelled in the FEM sub-assemblies, and instead, tie constraints were used to model the welds. This is a reasonable modelling assumption, as the capacity design of these welds will ensure

their elastic response. This is a widely accepted assumption in practice and research [5], [25] [27]. Also, global buckling of the girder is prevented due to bracing provided by beams.

4.3 Benchmarking with HE-RWS connection by Davarpanah et al.

The specimen is an RWS connection with a horizontal elliptical opening in the beam web (HE-RWS) [5]. An IPE270 was used for the girder and an IPB200 for the column. Connection details, such as the doubler plate, continuity plate dimension, and weld properties, followed the tested prototype. The connection sections were made of grade ST37 Iranian steel (similar to S235 in the European standard). The modelling approach was initially benchmarked by simulating the experimental study by Davarpanah and his collaborators, as shown in Figure 7.

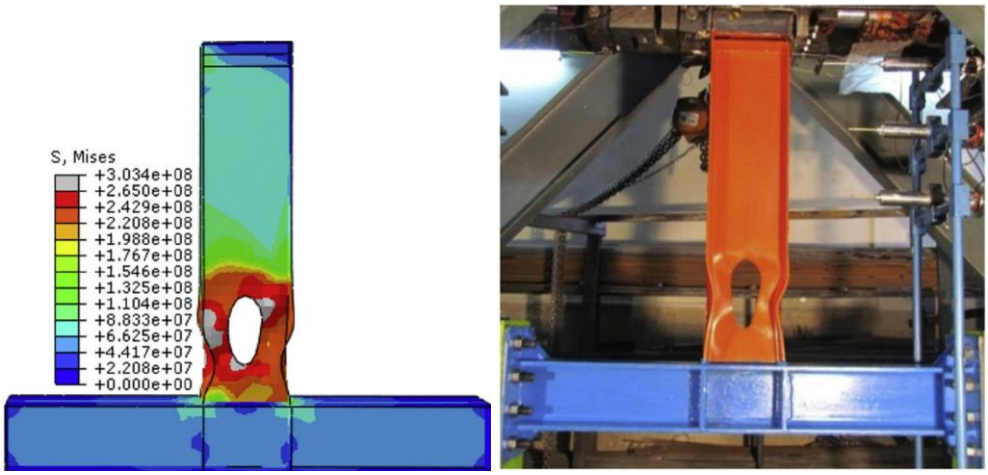

Figure 7: Distribution of Von Mises stress and Local buckling of the flange in the FE: (a) HE-RWS Von Mises stress (b) HE-RWS after testing

Figure 8 compares the outcomes (hysteresis curves) of the modelling scheme proposed in this study with the experimental results of Davarpanah's study (FEM curve plotted directly on top of the experimental curve from the literature). There is an acceptable agreement between the current FEM results compared to the experimental and FEM results in the mentioned study.

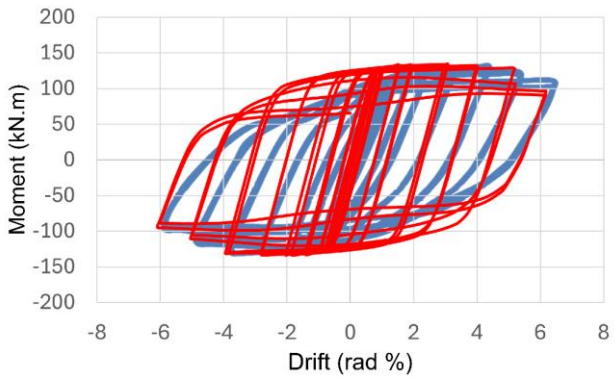

Figure 8: Comparison of the current FEM (in red) with the experimental study (in blue) by Davarpanah for the HE-RWS connection [5]

4.4 Mesh optimisation

The optimisation of the FE analysis involved comparing results from dense meshes (using 5mm elements) with sparser meshes (using 15mm and 20mm elements). The overall moment-rotation curves were practically similar for both mesh densities, even though the running computing time for the dense meshes was significantly longer. Hence, element sizes between 15mm and 20mm were adopted for the parametric analyses. **Table 2** presents the tabulated negative and positive maximum moments for benchmarking with Davarpanah's experimental results and that of FEA.

Table 2: Benchmarking with Davarpanah's experiment and FEA

Specimen	Max Moment (kN.m)		Error (%)	
HE-RWS (Experimental)	+131.4	-133.5	-	-
HE-RWS (FEA-Davarpanah)	+133.4	-134.1	1.5	0.44
HE-RWS (Mesh 15 mm)	+133.6	-132.9	1.67	-0.44
HE-RWS (Mesh 5 mm)	+127.6	127.4	-2.89	-4.56

It is crucial to highlight that the maximum moment *(M_m)* value has a low sensitivity to mesh size. However, its corresponding rotation, θ_m is sensitive. For instance, a change as small as 1 mm in mesh size can alter the value of θ_m. This sensitivity arises from the fact that the peak moment typically occurs during the larger cycles of the loading protocol while interstorey drift demands were already large. Such sensitivity is important when determining the peak points to define yield points using the idealised force-deformation method recommended in FEMA 356 [28]. Nevertheless, this issue was critical only when comparing the outcomes of the 20 mm and 15 mm element-size meshes, while becoming negligible as the results of the 5 mm element-size mesh were benchmarked against the 15 mm one. Henceforth, this element size was adopted hereinafter.

Benchmarking with DC-M connection by Nia et al.

To provide further reassurance, a second benchmarking assessment was carried out. This time, testing on a welded, unreinforced web connection to a box column (WUF-W) was considered [26]. The connection, which included shear tabs and continuity plates, was intended to represent a medium-sized multi-storey exterior connection. The tie command is used to model all welds. Kinematic coupling to a reference point simulated the load point and fixed column end arrangements. Further details of the connection and the experimental setup can be found in the literature [26].

The buckling of the flanges at a 6% drift is shown in **Figure 9**. Outcomes of the finite element model considered in this study can replicate the observed failure mode.

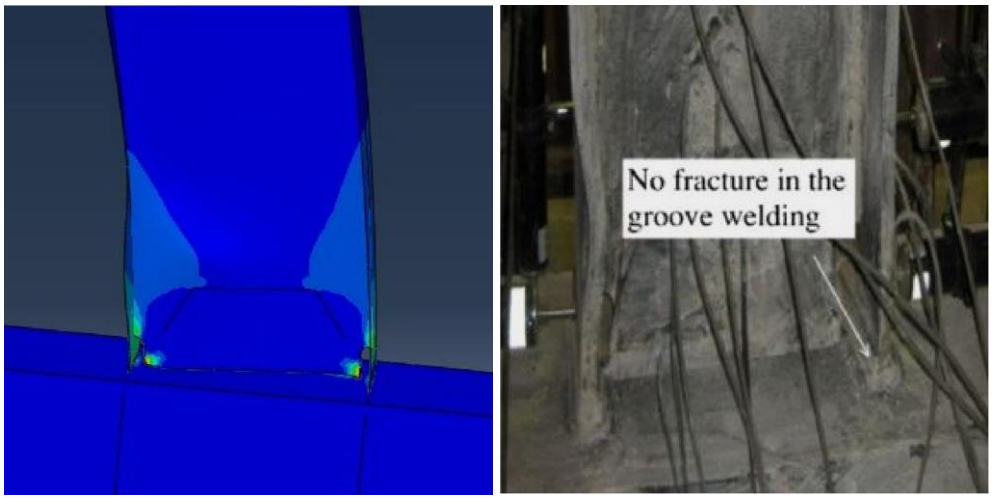

Figure 9: DC-M deformation of FE model ((PEEQ) contour plot) and experimental study, both at 6% drift

In addition, **Figure 10** compares the obtained hysteresis curves using the modelling approach of this study, with the results of the experiments and FEAs provided in Nia et al. The black solid curve is the outcome of this study's simulation. The blue and red curves represent the measured total forces (kN) at the tip of the beams and the rotations observed during the identical experiments conducted by Nia et al. [26].

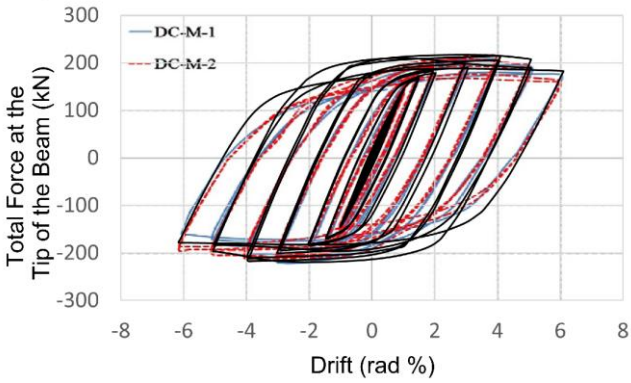

Figure 10: Comparisons of the current FEM result (in black) with those from two identical experiments conducted by Nia et al. for DC-M models *[26]*

Figure 10 indicates an appropriate fit between the results, verifying the current FE model's ability to predict the strength degradation by local buckling in the plastic hinge region. Ultimately, the FEM developed in this study employs a single Python script in ABAQUS capable of accurately representing the moment-rotation hysteretic curves for two entirely different experiments with varying properties and geometries.

5. Parametric Analysis

After FEM validation, the material properties of HE-RWS presented in **Table 1** are selected for parametric studies. A parametric study of 90 specimens with fixed beams with isolated web openings was carried out. The models are IPE270 beams with web opening geometry parameters, as shown in **Figure 3**, ranging from *0.30h* to *0.75h*, along with nine *S* variations spanning *0.40h* to *2h* for each beam. These specifications are reasonable for low-rise buildings, considering bay widths ranging between 3.5m to 4m, leading to span/height ratios between 12 to 15. **Table A1** shows the beam properties and RWS parameters used in FEA, while Figure the table illustrates the PEEQ and corresponding Von Mises for all cases. Key outcomes from this parametric study include the characterisation of backbone curves, computation of PEEQ and Von Mises strains, yield, peak and ultimate moments discussed in Section 2, besides determining which combinations of S and d_o result in yielding only in the protected zone.

The equivalent plastic strain index (PEEQ) is one of the most effective parameters for determining the likeness of the connection assembly being brittle or ductile and has been used by researchers as a criterion of plastic strain demand [29] [30]. Thus, this index is considered a scale for measuring the local inelastic strain demand [31]. The PEEQ index values are used to determine the location of the plastic hinge under cyclic loading conditions [32]. An increase in the PEEQ index for a specific location indicates a higher possibility of cracking, damage, or

deformation occurring in that region [32]. In addition, another study showed that high PEEQ values indicate a high likelihood of fracture due to tearing at a relatively low drift angle [33]. Complimentarily, FEMA 350 has highlighted that when the plastic hinge forms in the beam at the face of the column, this can result in large inelastic strain demands on the weld metal and surrounding heat-affected zones. These conditions can lead to brittle failure [3]. Hence, the PEEQ distributions are also considered to evaluate whether inelasticity initiates into the beam web within the designated protected zone away from the column face; therefore, protecting welds and fragile components from inelastic action. It is expected that providing appropriate combinations of S and d_o should lead to low inelastic action at the beam-column interface, hence attaining low PEEQ values there.

All models consider a fixed beam (encastré) at the column face, thereby all six degrees of freedom are restrained. While, cyclic drift demands are applied at the inflection point of the beam in both Scenarios, in accordance with AISC 341 [17]. In detail, it is applied 35mm from the top of the beam. The imposed drift time history is taken up to two cycles of 0.06 rad with increments of 0.01 rad, as shown in **Figure 1**. It must be highlighted that drift capacity outcomes are lower-bound estimates as they neglect column and joint deformations. Capacity design of these elements can be calculated once overstrength factors have been computed for the fixed-on-the-column paradigm being considered. Once capacity design is enforced, plastic behaviour will be confined to protected zones, namely the vicinity of the perforations, hence keeping elastic behaviour on columns and joints. Likewise, initial imperfections are a secondary concern for this study as the emphasis is made on low-rise buildings with welded hot-rolled short span beams, which have relatively stocky beams and columns. The archetypal model is shown in **Figure 11**. Appendix A (**Figure A4**) illustrates an example of the displacement time history, developed in accordance with the AISC 341 loading protocol [17], that is shown in **Figure 1** and applied to the subassembly depicted in **Figure 11**.

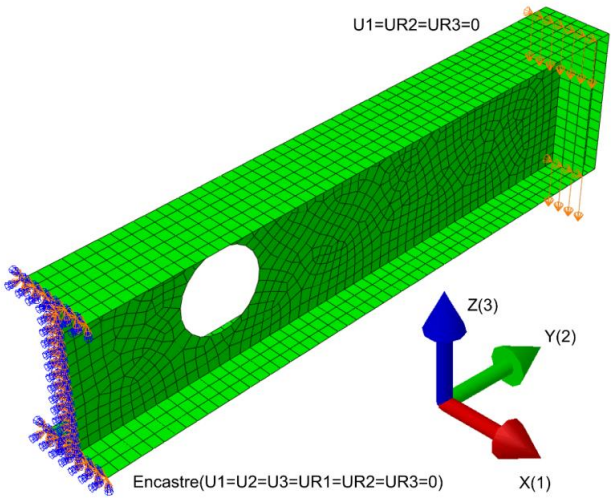

Figure 11: Typical FEM model considered in the parametric analyses

5.1 Yield moment

The effective yield moment was initially estimated considering Equations (1) and (2). However, it was found that for most cases (56%), the maximum moment capacity does not exceed the theoretical plastification moment, regardless of the fact that stable hysteresis loops were obtained, and plasticity was constrained around the perforation. Hence, achieving acceptable behaviour considering capacity design principles. The reason for this outcome is an early development of the Vierendeel mechanism on the edges of the perforation, that limited extensive plastic action at the reduced cross-section. It must be stressed that 75% of compliant specimens showcased a maximum moment larger than 90% of the effective yielding moment, making results reliable.

Yet, there is a need to adopt a better definition of the effective yield moment as a significant share of capacity design-compliant cross sections will not achieve it. After reviewing diverse options, the most efficient alternative was taking an offset of 0.2% radians of the slope of the moment/rotation curve (i.e. the elastic moment/rotation stiffness). Then, the yield moment was defined at the intersection of the offset and the hysteresis curves, as shown in **Figure 12**.

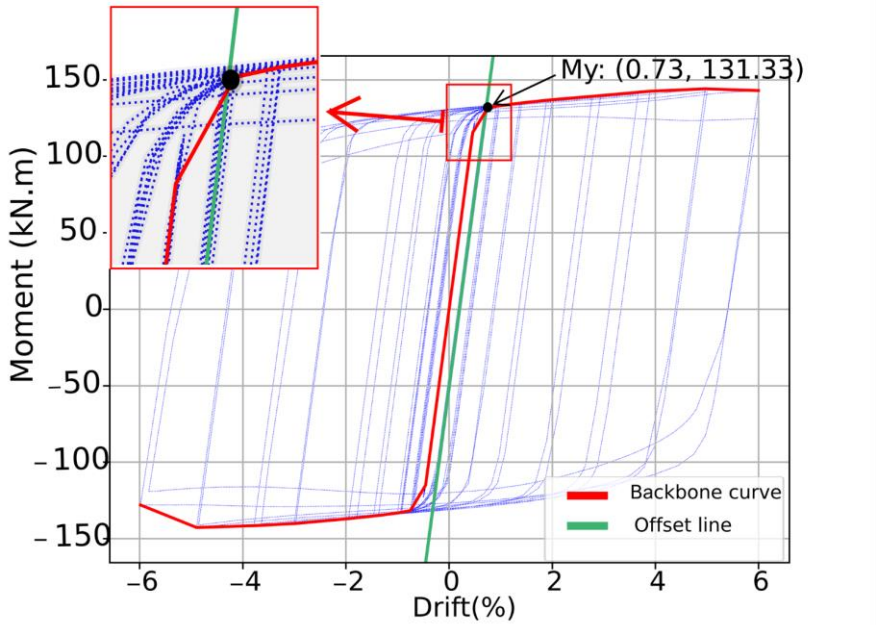

Figure 12: 0.2% drift offset approach for definition of the effective yield moment

As it is demonstrated (in Appendix B) the 0.2% drift offset method leads to a stiffness degradation of less than 20% at the effective yield, akin to the 20% limit on strength degradation for acceptance of the connection [17]. Thereby, this definition was adopted in this study and the effective yield moment M_y will be defined this way hereinafter.

Figure 13 displays changes in the yield moment M_y with varying parameters S and d_o for the 90 combinations. The results evidently showed that S has a mild effect on the yield moment, while d_o is the dominant parameter. Particularly, there is a reduction in the moment capacity by more than 52% for the case with the largest perforation (75% of the beam height) compared with a solid beam (without perforation).

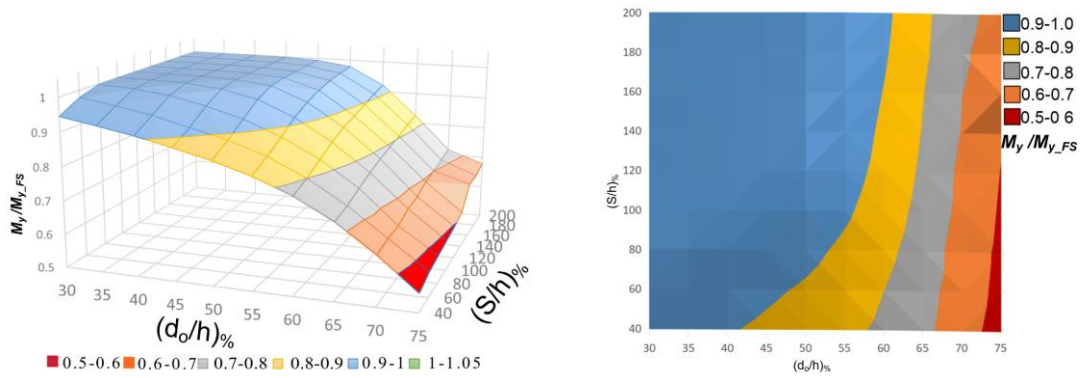

Figure 13: The effect and the interaction of (S and d_o) on the yield moment reduction (normalised) for 90 circular RWS connections (left figure: 3D view, right figure: Top view)

Also, the effective yield moment does not necessarily match the theoretical plastic moment (Equation 1). This outcome was previously observed in the literature [34]. One of the reasons is that the RWS connections may exhibit different yielding mechanisms depending on S and d_o as stated in Section 3. Therefore, a least-square nonlinear regression was performed to assess the variability of the yielding moment capacity in terms of the geometrical parameters of the RWS connection. It leads to the following value for the expected value of the ratio of observed effective yield moment and the theoretical plasticisation value:

$$\frac{M_y}{M_p} = 1.0631 - 0.4607\frac{d_o}{h} + 0.5803\frac{s}{h} - 0.7395\,\frac{d_o}{h}\,\frac{s}{h} \tag{5}$$

With a standard deviation of 0.028. Note that negative values are not allowed. However, they are extremely unlikely for reasonable values of d_o/h and S/h (within 0.35 and 0.75 for the former and 0.5 and 2 for the latter). Equation (5) has an explained variance R^2 of 0.86. Lower bound suggested design values (taken at minus one standard deviation) are:

$$\frac{M_{yD}}{M_p} = C_{yD} = 1.0351 - 0.4607\frac{d_o}{h} + 0.5803\frac{s}{h} - 0.7395\frac{d_o}{h}\frac{s}{h} \tag{6}$$

5.2 Maximum moment and static overstrength

Normalised peak moment values by the capacity of the solid IPE270 beam are shown in **Figure 14**. In these figures, a reduction of 52% in the moment capacity can be observed between the lower and upper limit values of the parameter d_o. However, only a reduction of 25% is observed in the peak moment when assessing S solely.

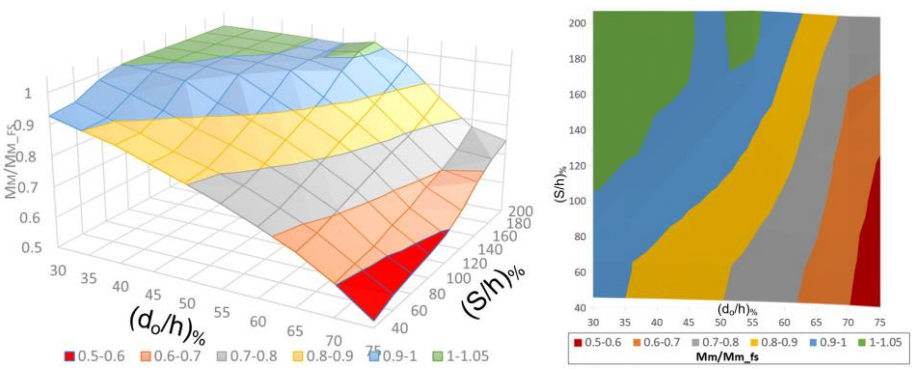

Figure 14: The effect and the interaction of 90 (S and d_o) combinations on the maximum moment strength reduction (normalised peak moment compared to that of the solid beam)

These trends are explicitly quantified when formulating analytical expressions for the static overstrength factor, namely the ratio between the yield moment and the maximum observed moment capacity. This parameter is critical for scaling shear and tensile demands for components outside the protected zone, thus ensuring that inelastic action is averted in them. Thus, a least-square nonlinear regression was effectuated to estimate the expected value of the overstrength factor (Equation (7)).

$$\frac{M_{max}}{M_y} = \Omega_s = 1.4940 - 1.5461\frac{d_o}{h} - 0.1517\frac{S}{h} + 1.2940\left(\frac{d_o}{h}\right)^2 + 0.1546\frac{d_o}{h}\frac{S}{h} + 0.0595\left(\frac{S}{h}\right)^2 \qquad (7)$$

While its explained variance R^2 is 0.93, negative values are not allowed, yet they are extremely unlikely for reasonable values of d_o/h and S/h ratios whose limits had been already stated. We recommend adopting an upper bound limit (at one standard deviation away) for design values, hence:

$$\Omega_{sd} = 1.5090 - 1.5461\frac{d_o}{h} - 0.1517\frac{S}{h} + 1.2940\left(\frac{d_o}{h}\right)^2 + 0.1546\frac{d_o}{h}\frac{S}{h} + 0.0595\left(\frac{S}{h}\right)^2 \qquad (8)$$

5.3 Compliance with capacity design principles

Capacity design requires that inelastic action is clustered within designated locations in the beam-column connections, designated as protected zones [17]. For RWS connections, these are over the immediate vicinity of the web perforations. Checking for inelastic behaviour was done by assessing contour plots of Von Mises stresses and Plastic Strain Equivalent. It is observed that large openings ($d_o/h > 0.65$) are capable of avoiding inelastic action in the beam-column interface, joint plates, and critical welds. Still, they reduce the moment capacity of the connection significantly (more than 20% following Equation (3)). This outcome was observed even for the shortest distance from the column (*0.35h*). However, other combinations of *S* and d_o successfully achieve this outcome with lesser moment reduction capacity. All combinations of d_o and *S* parameters that allow for compliance with capacity design principles are outlined in **Table 3**. An example illustrating how a suitable combination of *S* and d_o produces the RWS mechanism capable of moving the plastic hinge away from the column face is shown in Figure A3 in Appendix A.

Table 3: Successful combinations of (*S* and d_o) resulting in compliant RWS mechanism. (All FE models are listed in Table A1 and are shown in Figure A1)

(S/h) *%*	***(d₀/h)*** *%*									
	30	**35**	**40**	**45**	**50**	**55**	**60**	**65**	**70**	**75**

40	-	C2	C3	C4	C5	C6	C7	C8	C9	C10
60	-	C12	C13	C14	C15	C16	C17	C18	C19	C20
80	-	-	C23	C24	C25	C26	C27	C28	C29	C30
100	-	-	-	C34	C35	C36	C37	C38	C39	C40
120	-	-	-	-	C45	C46	C47	C48	C49	C50
140	-	-	-	-	-	C56	C57	C58	C59	C60
160	-	-	-	-	-	C66	C67	C68	C69	C70
180	-	-	-	-	-	-	C77	C78	C79	C80
200	-	-	-	-	-	-	C87	C88	C89	C90

Results presented in **Table 3** allow for formulation of a criterion for identifying if a particular RWS connection is capable of compliance with capacity design principles. For that purpose, logistic regression was effectuated to estimate the probability of obtaining a stable Vierendeel failure mode around the perforation (and thus ensuring compliance with capacity design). The following expression was found (**Figure 15**):

$$P_A = \frac{1}{1 + e^{-y}} \tag{9}$$

$$2.0131x10^{-5} = 0.2543\left(\frac{S}{H}\right)_{\%} - 0.2977\left(\frac{d_o}{H}\right)_{\%} - 0.029\left(\frac{S}{H}\right)_{\%}\left(\frac{d_o}{H}\right)_{\%} \tag{10}$$

Where P_A is the probability of avoiding yielding outside the protected zone. S/h and d_o/h ratios must be expressed as percentages. Equations (9) and (10) lead to a receiver operating characteristic (ROC) area under the curve of 0.99, thus making them reliable for design. Likewise, the outermost point from the origin of the ROC curve is observed for a median value (50% probability of being exceeded). Hence, this study suggests that taking a P_A value larger than the 50th percentile is reasonable for characterising a connection as acceptable for seismic applications. The limit state will be observed for the curve:

$$2.0131x10^{-5} = 0.2543\left(\frac{S}{H}\right)_{\%} - 0.2977\left(\frac{d_o}{H}\right)_{\%} - 0.029\left(\frac{S}{H}\right)_{\%}\left(\frac{d_o}{H}\right)_{\%} \tag{11}$$

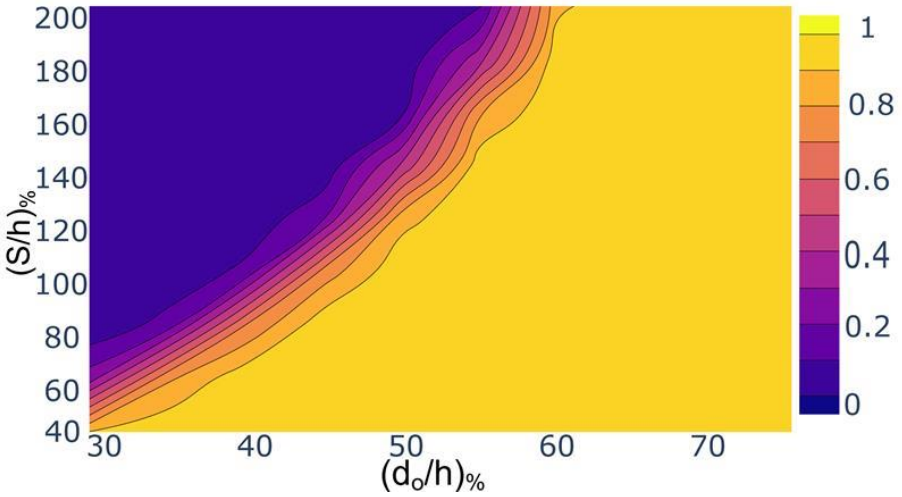

Figure 15: Probability of having yielded solely in the protected zone, for diverse *S* (abscissa) and d_o (ordinate)

5.4 Rotation capacity and strength degradation

Results of the parametric assessments indicate that all acceptable specimens following criteria presented in Section 5 showcase a highly ductile behaviour. Peak moment is always larger than 80% of the maximum values for drifts less than 0.04, hence allowing for deployment of connections within Special Moment Frames, per AISC 341 regulations [17]. As shown in **Figure 16**, this is the case for a large number of web openings and spacings, thus allowing for diverse design alternatives.

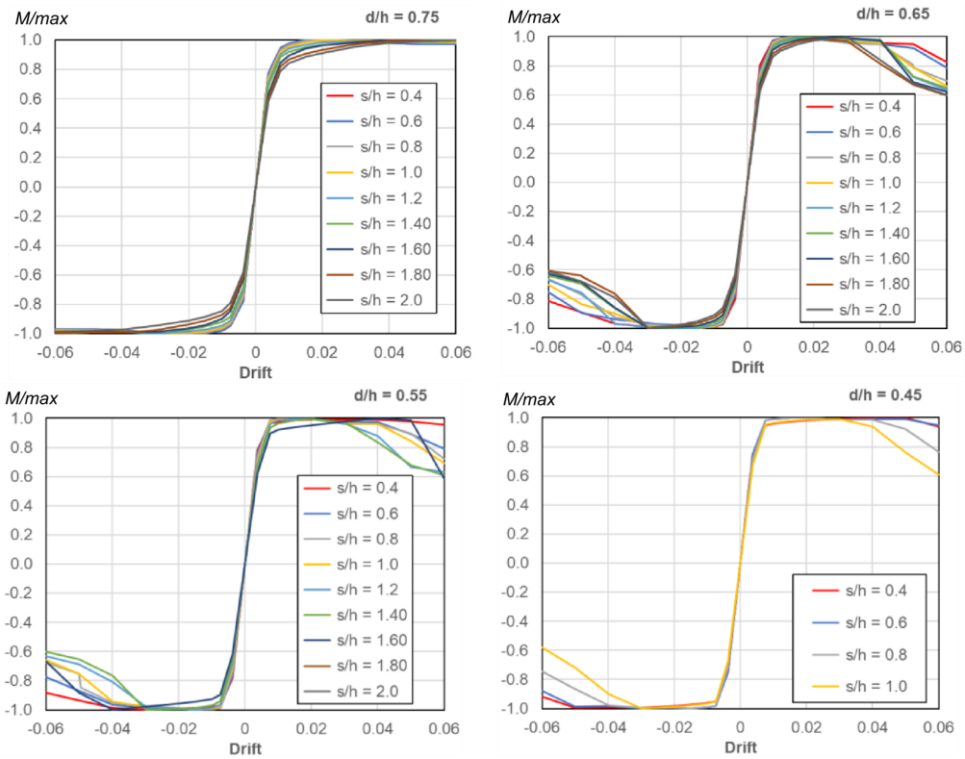

Figure 16: Backbone curves for specimens with d_o/h = 0.75, 0.65, 0.55, 0.45

Furthermore, if the ratio S/h is lower than 1.0, strength degradation can be limited to less than 10% for all cases. Even for large openings (d_o/h ratios) 6% drift demands can be reached with negligible loss of moment capacity. However, this comes with the drawback of a low yield moment. It can be beneficial for cases where beam-column welds are relatively weak, as shear demands can be capped. Moreover, hysteresis cycles of several specimens showcase large area, stable hysteresis loops. Note how there are gentle transitions on stiffness, thus precluding ringing and pinching. Likewise, origin wandering is negligible, indicating that there is no strain accumulation in a particular direction as long drift demands are symmetric. This further supports the fact that inelastic action is clustered within the protected zone.

6. Concluding Remarks

This study confirms that Reduced Web Section (RWS) connections are a plausible solution for seismic retrofit of buildings when RWS geometric parameters are chosen appropriately. Detailed parametric finite element model simulations indicate that they are capable of enduring 4% drift demands while showcasing stable hysteresis cycles. Likewise, in all cases assessed where yielding is inhibited outside the protected zone, strength reduction beyond 4% drift demands was less than 20%. This indicates that RWS connections are a ductile solution that can be deployed within special moment frames according to AISC [17].

Also, appropriate combinations of opening diameters d_o and web spacings from the column face S that led to plastic actions only in the protected zone (i.e. in the vicinity of the perforation) were found. This led to the formulation of an analytical expression for estimating the probability of yielding avoidance outside the protected zone, for given S and d_o values. Moreover, design combinations following capacity design principles can be proposed by considering a median (50th percentile) threshold. Likewise, results allowed for the derivation of analytical expressions in terms of d_o and S to define overstrength factors. They are key to account for increased shear and tensile demands outside the protected zone. It is recommended to adopt one plus standard deviation values for design. Henceforth, an analytical expression is provided for that purpose.

Overall, beams with end distance from the column face to the centreline of the perforation less than one times the beam's depth, and opening diameter less than half the beam's depth, can be expected to develop moments more than 80% of the capacity of solid beams, while inelastic

stresses developed away from the welding connection zone (within the pre-allocated zone). Additionally, they will be able to sustain more than 85% of the peak moment for drifts larger than 4%. Beams with larger web openings can reach 6% drifts without significant strength degradation. However, effective yielding moments can be significantly lower than the capacity of their unperforated (solid) counterparts when the web opening position is inappropriate as shown in **Figure 15**. In this case, the capacity reduction can be useful for retrofitting of buildings where shear transfer can be compromised due to the relaxed adoption of sound seismic capacity design principles for elements outside the protected zone.

Consequently, this study hints that use of RWS connection for seismic retrofit is plausible, particularly where shallow fully welded beams are employed in the lateral load resistance systems. Focus was made on one steel beam profile (IPE270), because it allows for testing in moderate-scale facilities; yet it can be deployed in lateral-load resisting frames with bay widths spanning 3m to 4 m. Moreover, welding to the column was considered instead of bolting. This choice is reasonable as transfer of large tensile and compressive couple actions requires the provision of many bolts that lead to the allocation of large end-plates to accommodate them. Henceforth, it is expected that low-depth, fully welded beams are more prevalent in low-scale dwellings, which in turn can be expected to be less compliant with capacity design principles.

It must be remarked that the outcomes of the study consider low-height buildings with relatively small spans, for which initial imperfections are not expected to be highly relevant, particularly when compared to the effects of overstrength. Moreover, conclusions should be further validated by experimental testing, which is now feasible as overstrength factors can be estimated. In detail, modelling and assessment of effects of initial imperfections should be done considering cruciform specimens where cross-sections of columns and properties of joints are adjusted by overstrength factors, to ensure that inelastic action only occurs on the protected zone (i.e. the vicinity of the perforation).

References

[1] World Steel Association, *Sustainability performance of the steel industry 2004-2022*. NA, 2023. [Online]. Available: https://worldsteel.org/steel-topics/sustainability/sustainability-indicators-2023-report/

[2] M. D. Alba-Rodríguez, A. Martínez-Rocamora, P. González-Vallejo, A. Ferreira-Sánchez, and M. Marrero, 'Building rehabilitation versus demolition and new construction: Economic and environmental assessment', *Environmental Impact Assessment Review*, vol. 66, pp. 115–126, Sep. 2017, doi: 10.1016/j.eiar.2017.06.002.

[3] FEMA 350, *Seismic Design Criteria for New Steel Moment Frame Buildings*, NA., NA vols. in NA, no. NA. NA: NA, 2001. [Online]. Available: https://ascelibrary.org/doi/abs/10.1061/40558%282001%29149

[4] C.-M. Uang and M. Bruneau, 'State of the art review on seismic design of steel structures', *J. Struct. Eng.*, vol. 144, no. 4, p. 03118002, Apr. 2018, doi: 10.1061/(ASCE)ST.1943-541X.0001973.

[5] M. Davarpanah, H. Ronagh, P. Memarzadeh, and F. Behnamfar, 'Cyclic behavior of welded elliptical-shaped RWS moment frame', *Journal of Constructional Steel Research*, vol. 175, p. 106319, Dec. 2020, doi: 10.1016/j.jcsr.2020.106319.

[6] M. A. Aschheim, 'MOMENT-RESISTANT STRUCTURE, SUSTAINER AND METHOD OF RESISTING EPISODIC LOADS', 6,012,256, Jan. 2000 [Online]. Available: https://patents.google.com/patent/US6012256A/en

[7] K. D. Tsavdaridis and T. Papadopoulos, 'A FE parametric study of RWS beam-to-column bolted connections with cellular beams', *Journal of Constructional Steel Research*, vol. 116, pp. 92–113, Jan. 2016, doi: 10.1016/j.jcsr.2015.08.046.

[8] Konstantinos Daniel Tsavdaridis and Theodore Papadopoulos, 'Assessment of Beam-Column Connections Using Perforated Beams with Multiple Closely Spaced Web Openings', *JCSR*, 2022, doi: 10.31224/2258.

[9] G. Vesmawala and R. Mehta, 'Analysis of steel beam column connection under cyclic loading with reduced web opening type fuses', *Asian J Civ Eng*, vol. 25, no. 3, pp. 2587–2597, Apr. 2024, doi: 10.1007/s42107-023-00930-9.

[10] D. T. Naughton, K. D. Tsavdaridis, C. Maraveas, and A. Nicolaou, 'Pushover Analysis of Steel Seismic Resistant Frames with Reduced Web Section and Reduced Beam Section Connections', *Front. Built Environ.*, vol. 3, p. 59, Oct. 2017, doi: 10.3389/fbuil.2017.00059.

[11] M. Shin, S.-P. Kim, A. Halterman, and M. Aschheim, 'Seismic toughness and failure mechanisms of reduced web-section beams: Phase 2 tests', *Engineering Structures*, vol. 141, pp. 607–623, Jun. 2017, doi: 10.1016/j.engstruct.2017.03.046.

[12] S. Momenzadeh, M. T. Kazemi, and M. H. Asl, 'Seismic performance of reduced web section moment connections', *Int J Steel Struct*, vol. 17, no. 2, pp. 413–425, Jun. 2017, doi: 10.1007/s13296-017-6004-x.

[13] K. D. Tsavdaridis, C. K. Lau, and A. Alonso-Rodríguez, 'Experimental behaviour of non-seismical RWS connections with perforated beams under cyclic actions', *Journal of Constructional Steel Research*, vol. 183, p. 106756, Aug. 2021, doi: 10.1016/j.jcsr.2021.106756.

[14] Afshin Moslehi Tabar, A. Alonso-Rodriguez, and K. D. Tsavdaridis, 'Building retrofit with reduced web (RWS) and beam (RBS) section limited-ductility connections', *Journal of Constructional Steel Research*, vol. 197, p. 107459, Oct. 2022, doi: 10.1016/j.jcsr.2022.107459.

[15] Mark Lawson and S J Hicks, 'DESIGN OF COMPOSITE BEAMS WITH LARGE WEB OPENINGS', *SCI PUBLICATION P355*, [Online]. Available: https://www.steel-sci.com/

[16] S. S. Fares, J. Coulson, and D. W. Dinehart, *Castellated and Cellular Beam Design*, 2017. [Online]. Available: https://www.aisc.org/Design-Guide-31-Castellated-and-Cellular-Beam-Design

[17] AISC 341-16, 'Seismic Provisions for Structural Steel Buildings', *American Institute of Steel Construction*, Jan. 2016, doi: NA.

[18] *Eurocode 3: Design of Steel Structures–Part 1–8: Design of Joints*, 2005. doi: NA.

[19] K. Weynand, J.-P. Jaspart, and M. Steenhuis, 'The stiffness model of revised annex j of eurocode 3', in *Connections in Steel Structures III*, Elsevier, 1996, pp. 441–452. doi: 10.1016/B978-008042821-5/50100-0.

[20] S. M. Mojtabaei, J. Becque, and I. Hajirasouliha, 'Behavior and Design of Cold-Formed Steel Bolted Connections Subjected to Combined Actions', *J. Struct. Eng.*, vol. 147, no. 4, p. 04021013, Apr. 2021, doi: 10.1061/(ASCE)ST.1943-541X.0002966.

[21] D. T. Phan, S. M. Mojtabaei, I. Hajirasouliha, T. L. Lau, and J. B. P. Lim, 'Design and Optimization of Cold-Formed Steel Sections in Bolted Moment Connections Considering Bimoment', *J. Struct. Eng.*, vol. 146, no. 8, p. 04020153, Aug. 2020, doi: 10.1061/(ASCE)ST.1943-541X.0002715.

[22] J. Ye, S. M. Mojtabaei, I. Hajirasouliha, and K. Pilakoutas, 'Efficient design of cold-formed steel bolted-moment connections for earthquake resistant frames', *Thin-Walled Structures*, vol. 150, p. S026382311830942X, May 2020, doi: 10.1016/j.tws.2018.12.015.

[23] T. A. Horton, I. Hajirasouliha, B. Davison, and Z. Ozdemir, 'More efficient design of reduced beam sections (RBS) for maximum seismic performance', *Journal of Constructional Steel Research*, vol. 183, p. 106728, Aug. 2021, doi: 10.1016/j.jcsr.2021.106728.

[24] T. A. Horton, I. Hajirasouliha, B. Davison, and Z. Ozdemir, 'Accurate prediction of cyclic hysteresis behaviour of RBS connections using Deep Learning Neural Networks', *Engineering Structures*, vol. 247, p. 113156, Nov. 2021, doi: 10.1016/j.engstruct.2021.113156.

[25] T. A. Horton, I. Hajirasouliha, B. Davison, Z. Ozdemir, and I. Abuzayed, 'Development of more accurate cyclic hysteretic models to represent RBS connections', *Engineering Structures*, vol. 245, p. 112899, Oct. 2021, doi: 10.1016/j.engstruct.2021.112899.

[26] Z. Saneei Nia, M. Ghassemieh, and A. Mazroi, 'WUF-W connection performance to box column subjected to uniaxial and biaxial loading', *Journal of Constructional Steel Research*, vol. 88, pp. 90–108, Sep. 2013, doi: 10.1016/j.jcsr.2013.04.008.

[27] Horton Thomas, 'Predicting Reduced Beam Section (RBS) Connection Performance in Steel Moment Frames', 2021. [Online]. Available: https://etheses.whiterose.ac.uk/29369/

[28] F. E. FEMA 356, 'Prestandard and commentary for the seismic rehabilitation of buildings', *Federal Emergency Management Agency: Washington, DC, USA*, 2000, [Online]. Available: https://www.nehrp.gov/pdf/fema356.pdf

[29] C.-C. Chen, C.-C. Lin, and C.-H. Lin, 'Ductile moment connections used in steel column-tree moment-resisting frames', *Journal of Constructional Steel Research*, vol. 62, no. 8, pp. 793–801, Aug. 2006, doi: 10.1016/j.jcsr.2005.11.012.

[30] L.-W. Lu, J. M. Ricles, C. Mao, and J. W. Fisher, 'Critical issues in achieving ductile behaviour of welded moment connections', *Journal of Constructional Steel Research*, vol. 55, no. 1–3, pp. 325–341, Jul. 2000, doi: 10.1016/S0143-974X(99)00092-9.

[31] S. El-Tawil and A. Member, 'Inelastic Behavior and Design of Steel Panel Zones', *ASCE*, pp. 183–193, 1998.

[32] R. Naseri, 'Numerical Assessment of the RBS Connection Reinforced with Stiffeners', Jun. 27, 2024, *In Review*. doi: 10.21203/rs.3.rs-4562032/v1.

[33] M. Davarpanah, H. Ronagh, P. Memarzadeh, and F. Behnamfar, 'Cyclic behaviour of elliptical-shaped reduced web section connection', *Structures*, vol. 24, pp. 955–973, Apr. 2020, doi: 10.1016/j.istruc.2020.02.016.

[34] K. Boushehri, K. D. Tsavdaridis, and G. Cai, 'Seismic behaviour of RWS moment connections to deep columns with European sections', *Journal of Constructional Steel Research*, vol. 161, pp. 416–435, Oct. 2019, doi: 10.1016/j.jcsr.2019.07.009.

[35] K. Priestley, ‘Displacement-Based Seismic Design of Structures’, *Earthquake Spectra*, vol. 24, no. 2, pp. 555–557, May 2008, doi: 10.1193/1.2932170.

Appendix A

Table A1: Summary table of 90 FEMs with fixed beams (θu and Mu of Non deteriorating models discussed in Section 2 in this table are ignored due to their unclear cyclic deterioration)

Click here for Interactive Version

Model	Area (mm^2)	(d_o/h) %	(S/h) %	M_y (FE) [kN.m]	M_y (AISC) [kN.m]	θ_m [rad]	M_m [kN.m]	$-\theta_m$ [rad]	$-M_m$ [kN.m]	θ_u [rad]	M_u [kN.m]	E_{diss} [kN.m]
FS	0	0	0	131.9	128.3	4	146.2	-4	-145.5	-	-	18.4
C-1	5150	30	40	124.7	125.4	4	135.6	-4	-134.6	-	-	17.8
C-2	7010	35	40	122.4	124.4	4	131.7	-4	-130.6	-	-	17.5
C-3	9156	40	40	119.7	123.2	5	128.1	-5	-127.2	-	-	17.2
C-4	11588	45	40	116.6	121.8	5	122.7	-3	-122.3	-	-	16.6
C-5	14306	50	40	113.1	120.3	4	117.4	-3	-118.6	-	-	16.1
C-6	17311	55	40	108.8	118.6	2	111.8	-3	-112.6	-	-	15.1
C-7	20601	60	40	103.1	116.8	2	105.2	-1.5	-105.0	-	-	14.0
C-8	24178	65	40	95.3	114.8	1.5	97.9	-1.5	-98.0	-	-	12.8
C-9	28040	70	40	85.1	112.6	1.5	88.2	-1.5	-87.9	-	-	11.9
C-10	32189	75	40	73.1	110.3	1.5	76.2	-1.5	-76.0	-	-	10.7
C-11	5150	30	60	129.1	125.4	6	137.2	-5	-135.6	-	-	18.6
C-12	7010	35	60	126.8	124.4	6	132.5	-3	-131.2	-	-	17.9
C-13	9156	40	60	124.3	123.2	5	128.3	-3	-127.5	-	-	17.3
C-14	11588	45	60	120.8	121.8	2	122.8	-3	-122.6	-	-	16.5
C-15	14306	50	60	117.2	120.3	1.5	118.6	-1.5	-118.8	-	-	15.5
C-16	17311	55	60	112.4	118.6	1.5	113.8	-1.5	-113.6	5.9	91	14.5
C-17	20601	60	60	105.6	116.8	1.5	107.1	-1.5	-106.9	-	-	13.7
C-18	24178	65	60	96.8	114.8	1.5	99.6	-1.5	-99.3	5.8	79.7	12.4
C-19	28040	70	60	86.3	112.6	1.5	89.7	-1.5	-89.5	-	-	11.6
C-20	32189	75	60	75.6	110.3	1.5	80.0	-1.5	-79.8	-	-	10.7
C-21	5150	30	80	131.6	125.4	4	143.1	-4	-142.2	-	-	18.8
C-22	7010	35	80	130.8	124.4	4	138.9	-4	-137.9	-	-	18.1
C-23	9156	40	80	129.1	123.2	4	133.9	-3	-133.7	5.7	107.1	16.7
C-24	11588	45	80	126.0	121.8	2	128.3	-1.5	-128.1	5.7	102.6	16.0
C-25	14306	50	80	122.1	120.3	1.5	123.9	-1.5	-123.8	5.7	99.1	15.3
C-26	17311	55	80	116.3	118.6	1.5	118.1	-1.5	-117.7	5.5	94.4	14.2
C-27	20601	60	80	109.0	116.8	1.5	111.3	-1.5	-111.1	5.6	89	13.5
C-28	24178	65	80	99.3	114.8	1.5	103.1	-1.5	-103.0	4.9	82.5	12.2
C-29	28040	70	80	86.4	112.6	1.5	90.8	-1.5	-90.8	-	-	11.7
C-30	32189	75	80	76.7	110.3	2	82.2	-3	-82.1	-	-	10.8
C-31	5150	30	100	131.9	125.4	4	146.4	-4	-145.6	-	-	18.8
C-32	7010	35	100	131.8	124.4	4	145.5	-4	-144.8	-	-	18.7
C-33	9156	40	100	131.4	123.2	4	143.4	-4	-142.4	-	-	18.4
C-34	11588	45	100	130.0	121.8	3	135.4	-3	-136.5	4.8	108.3	15.2
C-35	14306	50	100	126.8	120.3	2	130.0	-1.5	-130.0	4.7	104	14.6
C-36	17311	55	100	120.7	118.6	1.5	123.7	-1.5	-123.5	5.2	99	14.3
C-37	20601	60	100	112.2	116.8	1.5	115.7	-1.5	-115.9	4.8	92.6	13.2
C-38	24178	65	100	101.5	114.8	1.5	106.6	-1.5	-106.6	4.9	85.3	12.2
C-39	28040	70	100	88.7	112.6	2	94.0	-2	-93.8	5.8	75.2	11.7
C-40	32189	75	100	77.7	110.3	2	84.0	-3	-84.4	-	-	11.0
C-41	5150	30	120	131.9	125.4	4	146.5	-4	-145.5	-	-	18.8
C-42	7010	35	120	131.8	124.4	4	146.4	-4	-144.1	-	-	18.7
C-43	9156	40	120	131.7	123.2	4	145.9	-4	-145.5	-	-	18.7
C-44	11588	45	120	131.2	121.8	4	144.4	-4	-144.1	-	-	18.7
C-45	14306	50	120	129.6	120.3	3	136.5	-3	-137.7	-	-	18.7
C-46	17311	55	120	123.9	118.6	1.5	128.8	-1.5	-128.6	4.3	103.1	13.6
C-47	20601	60	120	114.9	116.8	1.5	120.5	-1.5	-120.7	4.5	96.4	12.7
C-48	24178	65	120	103.4	114.8	1.5	109.9	-1.5	-109.9	4.6	87.9	12.3
C-49	28040	70	120	89.3	112.6	2	95.8	-3	-95.8	5.7	76.6	11.7
C-50	32189	75	120	78.7	110.3	4	86.5	-3	-87.1	-	-	11.2

C-51	5150	30	140	131.9	125.4	4	146.5	-4	-146.0	-	-	18.8
C-52	7010	35	140	131.8	124.4	4	146.5	-4	-145.4	-	-	18.7
C-53	9156	40	140	131.8	123.2	4	146.2	-3	-141.7	-	-	18.6
C-54	11588	45	140	131.4	121.8	4	145.9	-4	-144.2	-	-	18.5
C-55	14306	50	140	130.4	120.3	4	144.5	-4	-144.5	-	-	18.6
C-56	17311	55	140	126.1	118.6	2	134.2	-3	-134.7	4.2	107.3	13.7
C-57	20601	60	140	116.5	116.8	1.5	124.2	-1.5	-124.0	4.6	99.3	13.0
C-58	24178	65	140	104.8	114.8	2	113.4	-3	-113.5	4.7	90.7	12.3
C-59	28040	70	140	91.5	112.6	4	99.7	-3	-100.1	5.4	79.8	11.7
C-60	32189	75	140	80.3	110.3	6	90.4	-6	-90.9	-	-	11.6
C-61	5150	30	160	131.9	125.4	4	146.4	-4	-146.2	-	-	18.8
C-62	7010	35	160	131.8	124.4	4	146.6	-4	-146.2	-	-	18.8
C-63	9156	40	160	131.7	123.2	4	146.5	-4	-145.7	-	-	18.7
C-64	11588	45	160	131.5	121.8	4	146.2	-4	-146.0	-	-	18.7
C-65	14306	50	160	130.7	120.3	4	145.5	-4	-145.3	-	-	18.7
C-66	17311	55	160	127.7	118.6	4	142.6	-4	-142.5	5.4	114	16.2
C-67	20601	60	160	118.3	116.8	2	128.9	-2	-128.1	3.9	103.1	12.7
C-68	24178	65	160	105.9	114.8	2	115.8	-3	-116.6	4.6	92.6	12.3
C-69	28040	70	160	92.4	112.6	4	102.5	-3	-102.5	5.2	82	11.8
C-70	32189	75	160	88.0	110.3	6	104.1	-6	-103.2	-	-	12.6
C-71	5150	30	180	131.9	125.4	4	146.4	-4	-145.6	-	-	18.7
C-72	7010	35	180	131.8	124.4	4	146.5	-4	-146.1	-	-	18.8
C-73	9156	40	180	131.7	123.2	4	146.5	-4	-145.8	-	-	18.7
C-74	11588	45	180	131.5	121.8	4	146.3	-4	-146.1	-	-	18.8
C-75	14306	50	180	130.9	120.3	4	145.7	-4	-145.6	-	-	18.6
C-76	17311	55	180	128.4	118.6	5	147.9	-4	-143.9	-	-	18.7
C-77	20601	60	180	120.2	116.8	3	134.1	-3	-134.9	4.4	107.2	13.3
C-78	24178	65	180	107.8	114.8	2	120.2	-3	-122.2	4.1	96.1	12.2
C-79	28040	70	180	93.5	112.6	4	106.9	-3	-105.7	5.4	85.5	12.2
C-80	32189	75	180	87.9	110.3	6	106.9	-6	-106.5	-	-	12.7
C-81	5150	30	200	131.9	125.4	4	146.5	-4	-146.0	-	-	18.8
C-82	7010	35	200	131.8	124.4	4	146.6	-4	-146.3	-	-	18.8
C-83	9156	40	200	131.8	123.2	4	146.5	-4	-146.2	-	-	18.8
C-84	11588	45	200	131.6	121.8	4	146.3	-4	-145.9	-	-	18.7
C-85	14306	50	200	131.0	120.3	4	145.8	-4	-145.7	-	-	18.6
C-86	17311	55	200	129.0	118.6	5	148.7	-5	-147.2	-	-	18.7
C-87	20601	60	200	121.5	116.8	4	139.8	-4	-139.5	4.6	111.8	14.5
C-88	24178	65	200	108.7	114.8	3	125.6	-3	-126.3	4.2	100.5	12.5
C-89	28040	70	200	94.6	112.6	4	110.4	-4	-109.3	5	88.3	12.2
C-90	32189	75	200	89.5	110.3	6	113.5	-6	-111.8	-	-	13.1

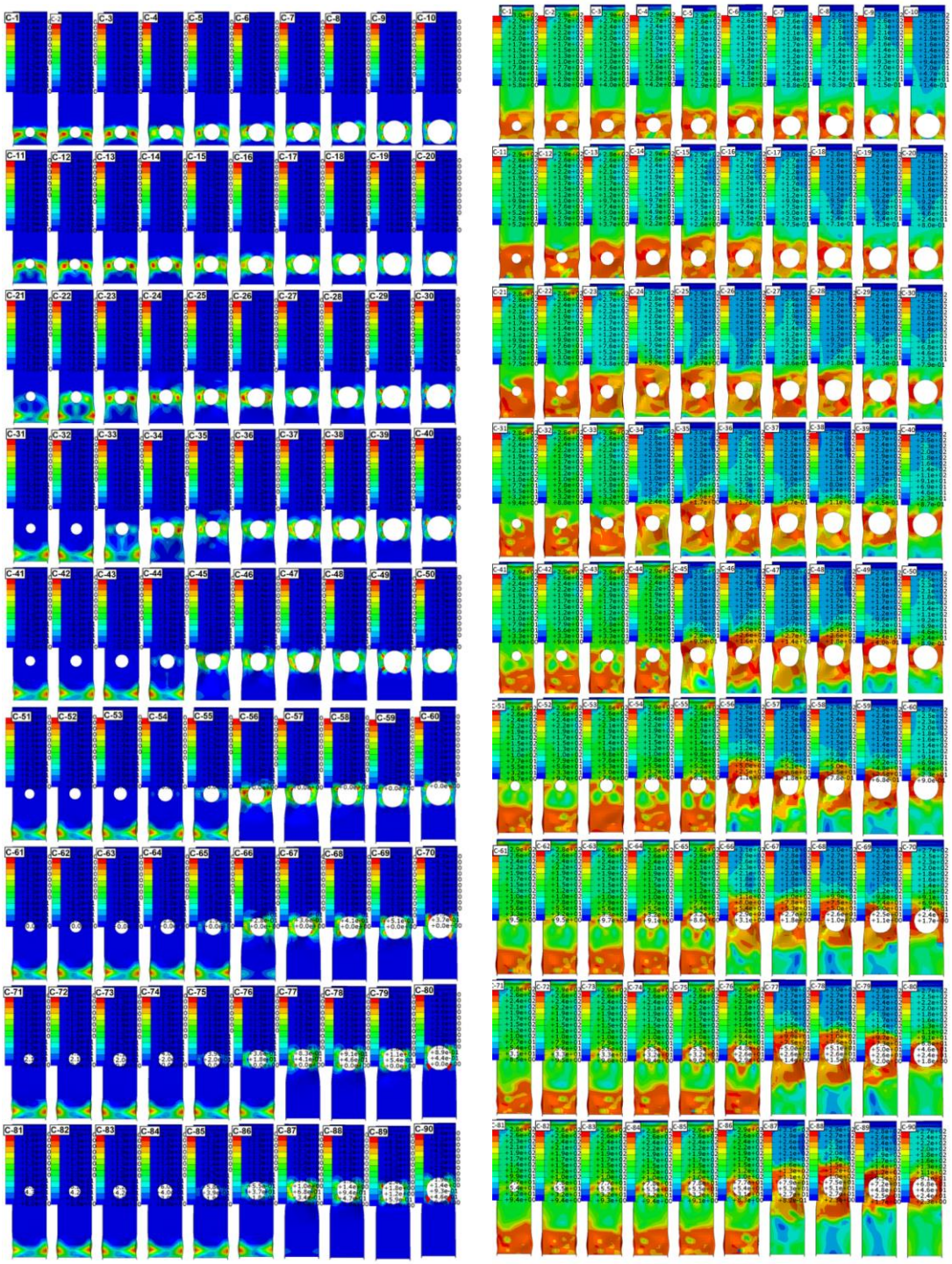

Figure A1: *Circular RWS behaviour with different (S and d_o) (90 combinations). (a) PEEQ for circular web openings. (b) Von Mises stresses stresses for circular web openings*

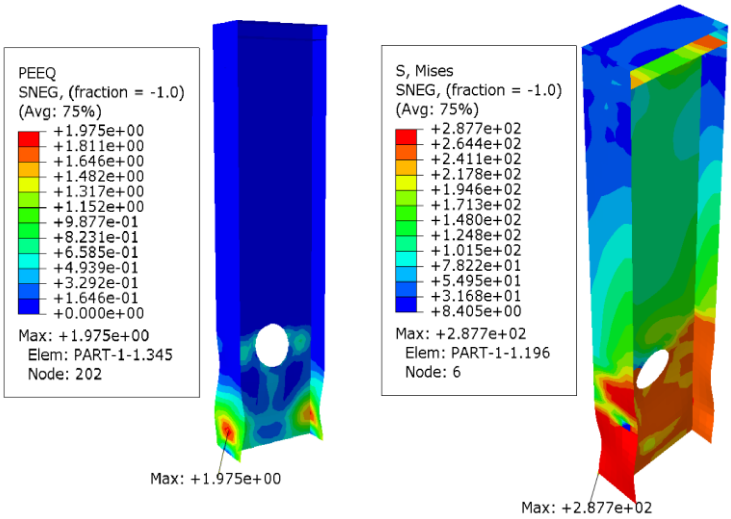

Figure A2: *Example of an unsuccessful RWS mechanism; Plastic hinge and high stress at the column face (Model C33 in Table 3)*

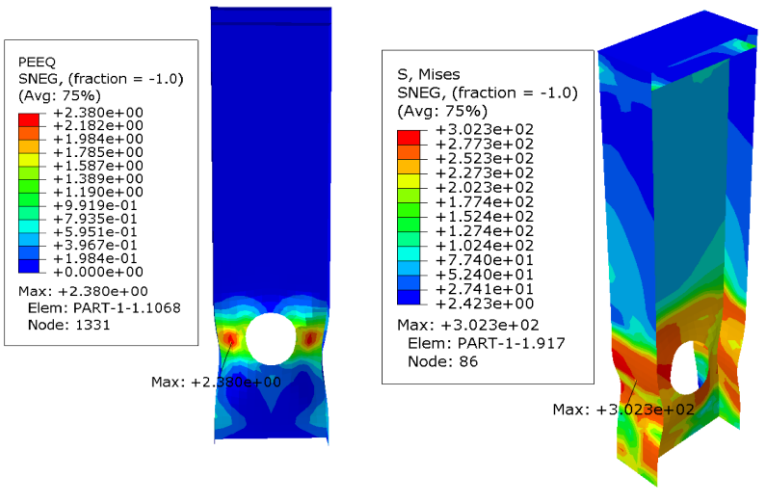

Figure A3: *Example of a successful combination of S and d_o resulting in RWS mechanism; Plastic hinge within the protected zone away from the column face*

(Model C34 in Table 3)

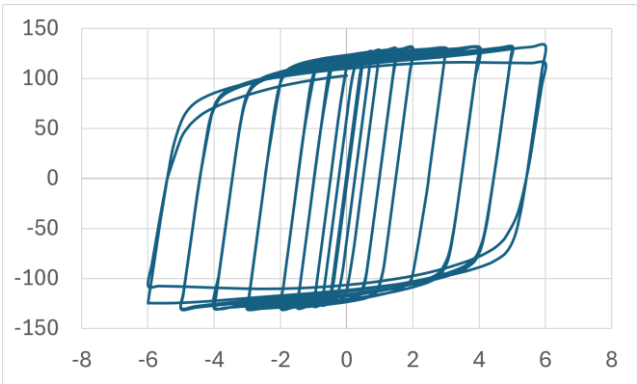

Figure A4: *Example of cyclic displacement diagram of a compliant RWS connection having RWS mechanism (Model C13 in Table 3)*

Appendix B: Offset method for definition of the effective yielding moment of RWS connections

Consider a close up of a backbone curve in the vicinity of the elastic region (constant moment-rotation stiffness). The figure outlines how the effective yield moment M_y is defined:

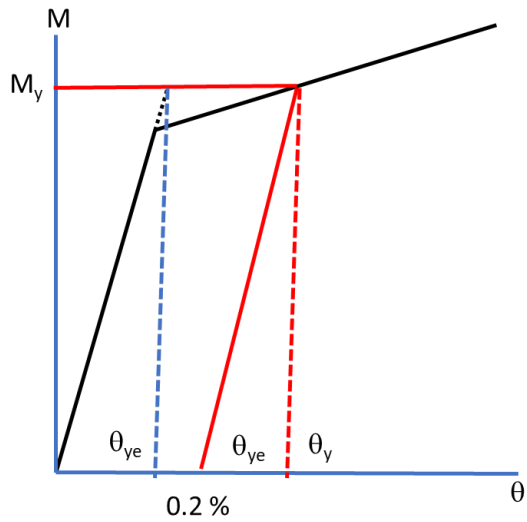

Figure B1: Outline of the yield moment method

$$M_y = k_e \theta_{ye} \tag{B.1}$$

While the secant moment-rotation stiffness when *My* occurs (at the intersection of the hysteresis curve and the offset) becomes:

$$k_{sy} = \frac{k_e \theta_{ye}}{\theta_{ye} + 0.02\%} \tag{B.2}$$

Then, it is possible to divide both sides of the equation by θ_{ye} to obtain the following expression:

$$k_{sy} = k_e \frac{1}{1 + \frac{0.2\%}{\theta_{ye}}} \tag{B.3}$$

A plausible lower bound estimate for θ_{ye} is 0.8% for A36 steel [35], leading to:

$$k_{sy} = k_e \frac{1}{1.25} = 0.8\, k_e \tag{B.3}$$

Then, the secant moment-rotation stiffness at the effective yielding can be expected to be equal or larger than 80% of the elastic moment-rotation stiffness.